Wind and Structures, Vol. 2, No. 4 (1999) 305-323
DOI: http://dx.doi.org/10.12989/was.1999.2.4.305

Comparison of several computational turbulence models with full-scale measurements of flow around a building

N.G. Wright† and G.J. Easom‡

School of Civil Engineering, The University of Nottingham, Nottingham, NG7 2RD, U.K.

Abstract. Accurate turbulence modelling is an essential prerequisite for the use of Computational Fluid Dynamics (CFD) in Wind Engineering. At present the most popular turbulence model for general engineering flow problems is the k-ε model. Models such as this are based on the isotropic eddy viscosity concept and have well documented shortcomings (Murakami *et al.* 1993) for flows encountered in Wind Engineering. This paper presents an objective assessment of several available alternative models. The CFD results for the flow around a full-scale (6 m) three-dimensional surface mounted cube in an atmospheric boundary layer are compared with recently obtained data. Cube orientations normal and skewed at 45° to the incident wind have been analysed at Reynolds number of greater than 10^6. In addition to turbulence modelling other aspects of the CFD procedure are analysed and their effects are discussed.

Key words: turbulence model; wind engineering; anisotropy; full-scale; bluff body; computational fluid dynamics; buildings; k-ε.

1. Introduction

Analysis of wind loading on buildings for design purposes has been carried out in wind tunnels for many years. Recently attention has started to focus on the use of computers for this purpose. With their ability to carry out large numbers of calculations on large amounts of data, they are well suited to solving the discretised versions of the laws governing fluid flow. However, there is still much doubt amongst the wind engineering community as to how successful the Computational Fluid Dynamics (CFD) approach can be. Some of this is based on concerns over the ability of the models to accurately represent the flows of interest and some is a result of early CFD work that was restricted by the power of computers and lack of understanding of the limitations of the technique. In this paper, work is presented that attempts, inter alia, to analyse one of the most important areas to be addressed in CFD for wind engineering, that is turbulence modelling. Rather than presenting one model and attempting to demonstrate its superior abilities, this work implements several and presents an analysis of their relative strengths and weaknesses in order to inform users of CFD in wind engineering. Previous work has often compared turbulence models with model-scale data from wind tunnels (Murakami

† Lecturer
‡ Postgraduate student

1993, Castro and Robbins 1977). In this paper comparisons of full-scale experimental data and numerically derived flowfields are presented.

The most accurate way to model fluid flow numerically is direct numerical simulation (Murakami 1997), which involves discretising the equations at a mesh size below the Kolmorogov length scale. For practical wind engineering flows, this is well beyond the capabilities of present day computers. Large Eddy Simulation (LES) attempts to overcome this limitation by calculating the larger eddies directly and accounting for ones below a fixed filter size through a model such as the Smagorinsky sub-grid model (Smagorinsky 1966). The authors have implemented this technique and an evaluation is ongoing. However, even LES has significant computing requirements and consequently turbulence models based on Reynolds averaging such as the k-ε and differential stress model (DSM) are commonly used in CFD. These models, referred to as Reynolds Averaged Navier-Stokes (RANS), calculate a mean, steady state velocity and pressure field and account for the velocity and pressure fluctuations through modelled variables. In the case of the k-ε model these are kinetic energy and its rate of dissipation and for DSM the six Reynolds stresses and the rate of dissipation of kinetic energy. Given the resource requirements of DNS and LES it is still necessary to use steady-state RANS models and it is likely to remain so for some time.

Wind engineering flows present several challenges to CFD practitioners and an appreciation of the difficulties is essential to making appropriate use of the results. Firstly, although the time averaged turbulence models mentioned above have been applied widely in CFD, their use in computational wind engineering is restricted by their difficulty in predicting time dependent phenomena. Furthermore flows around buildings are characterised by the presence of multiple recirculation zones embedded within a uni-directional flow. The resulting interactions between adjacent regions of separated and attached flow are difficult to simulate using equations for a single length and velocity scale. These modelling difficulties are compounded by the presence of streamline curvature and both favourable and adverse pressure gradients.

At present RANS turbulence modelling is one of the major sources of error in computational wind engineering. This paper presents a critical review of results from several models for the flow around a 6m surface-mounted cube in a fully developed atmospheric boundary layer. Comparisons with full-scale measurements obtained from a similar cube located at the Silsoe Research Institute are presented and some conclusions are drawn. Suggestions are made for the direction of future work in this area.

2. Theoretical aspects of the CFD

The computational work presented here uses a finite volume technique to solve the Reynolds-averaged Navier-Stokes equations. The computational domain is divided into blocks, each of which has its own boundary fitted, structured grid. The blocks are connected at the interfaces between them and the solution technique iterates over each block until a converged solution is obtained for the discretised equations.

Within a block the equation for each velocity component is solved sequentially and a derived pressure equation is solved according to the SIMPLE algorithm (Patankar and Spalding 1972). Various methods are available to solve the system of linear algebraic equations. This work uses Stones' Strongly Implicit method (Stone 1968) and an algebraic multigrid method (Webster 1998).

Two discretisations are used and a comparison and analysis is presented later.

The algorithms are implemented through the use of a commercially available code - CFX (CFX International 1997). This route was taken as opposed to the development of a bespoke code for several reasons:

- CFX, like other commercial codes, has been validated for many test cases in a number of different application areas.
- The tools for geometry building, mesh definition and the presentation and analysis of results are available and versatile.
- The code has many options for different models and solution algorithms.
- Transfer of results and recommendations to end-users is easily accomplished as the code is available for many computer platforms and there is comprehensive documentation and training.

Where necessary use is made of the ability to add user-defined FORTRAN subroutines to accomplish specific tasks and for more substantial alterations the University of Nottingham has access to the source code.

Several turbulence models are available in the standard release of CFX. Three of these were chosen for this work as a broad representation of those generally available. In addition the MMK model proposed in Tsuchiya *et al.* (1996), was incorporated by additional FORTRAN. The evaluation of these four was intended to highlight weaknesses and point to possible future development areas for turbulence modelling in full-scale computational wind engineering. The four models are described below.

2.1. *k-ε* model

The standard *k-ε* model of Launder and Spalding (Launder and Spalding 1974) is, at present, the most widely used turbulence model in CFD due to relatively low computational cost and good numerical stability. The model has two turbulence transport equations, one for the turbulent kinetic energy of the flow, Eq. (1) and one for the dissipation rate, Eq. (2). These equations are used to define a single velocity and length scale representative of large scale turbulence which are in turn used to define an additional 'turbulent' viscosity which is intended to represent the turbulence of the flow. The additional viscosity is incorporated into the Reynolds averaged Navier Stokes equations to represent the action of the Reynolds stresses through the Boussinesq hypothesis (Eq. 3).

$$\rho \frac{\partial k}{\partial t} + \rho U_j \frac{\partial k}{\partial x_j} = \tau_{ij} \frac{\partial U_i}{\partial x_j} - \rho\varepsilon + \frac{\partial}{\partial x_j}\left[(\mu + \mu_t/\sigma_k) \frac{\partial k}{\partial x_j} \right] \tag{1}$$

$$\rho \frac{\partial \varepsilon}{\partial t} + \rho U_j \frac{\partial \varepsilon}{\partial x_j} = C_{\varepsilon 1} \frac{\varepsilon}{k} \tau_{ij} \frac{\partial U_i}{\partial x_j} - C_{\varepsilon 2} \rho \frac{\varepsilon^2}{k} + \frac{\partial}{\partial x_i}\left[(\mu + \mu_t/\sigma_\varepsilon) \frac{\partial \varepsilon}{\partial x_j} \right] \tag{2}$$

$$\tau_{ij} = 2\mu_t S_{ij} - \frac{2}{3} \rho k \delta_{ij} \tag{3}$$

Each of the variables is defined at the end of the paper. Eq. (3) shows that the Reynolds stress tensor includes a 2/3 $\rho k \delta_{ij}$ term, so that a third of the turbulent kinetic energy is

allocated to each of the normal stresses. This isotropic assumption is carried through to both the momentum equations and the turbulent kinetic energy and energy dissipation equations. For example the first term on the right hand side of Eq. (1) (the production term) incorporates the Reynolds stress tensor τ_{ij}. The full production term for anisotropic turbulence, P_k, is as follows (in 2D for simplicity):

$$P_k = -\overline{u'u'}\frac{\partial \bar{u}}{\partial x} - \overline{w'w'}\frac{\partial \bar{w}}{\partial z} - \overline{u'w'}\frac{\partial \bar{u}}{\partial z} - \overline{w'u'}\frac{\partial \bar{w}}{\partial x} \tag{4}$$

This term gives P_k as the difference between the turbulence production from diagonal elements of the strain rate tensor and production from off-diagonal elements.

Using the continuity equation and then the eddy viscosity concept this equation gives (Murakami 1993):

$$P_{kn} = \left(-\overline{u'u'} - \overline{w'w'} \right) \frac{\partial \bar{u}}{\partial x} \tag{5}$$

and

$$P_{kn} = 4\nu_t \left(\frac{\partial \bar{u}}{\partial x} \right)^2 \tag{6}$$

When an anisotropic turbulence model is used, such as the differential stress model, P_{kn} is calculated using the form as described in Eq. (5) which involves two components. When using the eddy viscosity concept these two normal stresses cannot be incorporated so they are simply expressed as Eq. (6) by adding the two components of turbulence production (Murakami 1993). Hence the value of turbulent production is always large and positive. The consequences of this simplification will be investigated in this work.

2.2. RNG k-ε model

The RNG k-ε model (Yakhot *et al.* 1992) is derived from renormalisation group analysis of the Navier Stokes equations. This model is still based on the isotropic eddy viscosity concept and the Boussinesq hypothesis. It uses the standard k-ε model equations with the exception of revised model constants and a strain dependent term in the energy dissipation Eq. (7). The strain dependent term adjusts the rate of production of dissipation dependant on the rate of compressive strain in the fluid. This modifies the values of eddy viscosity. In areas of high compressive strain the production of dissipation is increased to counter the overproduction of turbulent kinetic energy, as a consequence of the isotropic eddy viscosity assumption, detailed earlier.

$$\rho\frac{\partial \varepsilon}{\partial t} + \rho U_j \frac{\partial \varepsilon}{\partial x_j} = (C_{\varepsilon 1} - C_{1\mathrm{RNG}})\frac{\varepsilon}{k}\tau_{ij}\frac{\partial U_i}{\partial x_j} - C_{\varepsilon 2}\rho\frac{\varepsilon^2}{k} + \frac{\partial}{\partial x_i}\left[(\mu + \mu_t/\sigma_\varepsilon)\frac{\partial \varepsilon}{\partial x_j} \right] \tag{7}$$

where

$$C_{1RNG} = \frac{\eta\left(1 - \frac{\eta}{\eta_0}\right)}{(1 + \beta\eta^3)} \tag{8}$$

and

$$\eta = \left(\frac{P}{\mu_t}\right)^{\frac{1}{2}} \frac{k}{\varepsilon} \tag{9}$$

η_0 and β are additional model constants.

2.3. MMK k-ε model

The MMK k-ε model (Tsuchiya *et al.* 1996) is a revision to the standard model to improve the k-ε model's performance specifically for wind engineering flow fields. The standard model constant C_μ becomes a variable that can reduce in magnitude dependent on the ratio of vorticity to shear. At flow impingement areas where the ratio is less than one a reduced value of C_μ is calculated thus reducing the eddy viscosity returned.

$$P_k = \nu_t s^2 \quad \text{where} \quad \nu_t = C_\mu \frac{k^2}{\varepsilon} \tag{10}$$

$$s = \sqrt{\frac{1}{2}\left(\frac{\partial \bar{u}_i}{\partial x_j} + \frac{\partial \bar{u}_j}{\partial x_i}\right)^2} \tag{11}$$

$$C_\mu = \begin{cases} C_\mu \dfrac{\Omega}{s} & \text{for } \dfrac{\Omega}{s} < 1 \\ C_\mu & \text{for } \dfrac{\Omega}{s} \geq 1 \end{cases}$$

This modification is intended to improve the prediction of turbulent kinetic energy and eddy viscosity for bluff body flowfields.

2.4. Differential stress model

The differential stress model of Launder, Reece and Rodi (1975) is a more complex model that solves individual transport equations for each of the six Reynolds stresses Eq. (12) and as such is an anisotropic turbulence model. In addition to the six Reynolds stress equations it solves an ε equation as with the k-ε model. The requirement to solve these extra transport equations leads to increased computational effort and in some cases reduced numerical stability. However, this can be offset by improved results for flows with significant anisotropic turbulence.

$$\frac{\partial}{\partial x_k}(\rho U_k \overline{u_i u_j}) = -\rho\left(\overline{u_j u_k}\frac{\partial U_i}{\partial x_k} + \overline{u_i u_k}\frac{\partial U_j}{\partial x_k}\right) + (\overline{u_i f_i} + \overline{u_i f_i}) + p\left(\overline{\frac{\partial u_i}{\partial x_j} + \frac{\partial u_j}{\partial x_i}}\right)$$

$$-2\mu\overline{\frac{\partial u_i}{\partial x_k}\frac{\partial u_j}{\partial x_k}} - \frac{\partial}{\partial x_k}\left(\rho\overline{u_i u_j u_k} + \overline{pu_i}\,\delta_{jk} + \overline{pu_j}\,\delta_{ik} - \mu\frac{\partial \overline{u_i u_j}}{\partial x_k}\right) \quad (12)$$

To account for the greater anisotropy near walls, extra terms known as 'wall reflection terms' can be used. There is no generic way of including these terms and they must be individually programmed into a model for each different geometry considered. The terms increase the instability of the solution technique and there is no agreement on how important these terms are (Murakami *et al.* 1993) for accurate solutions. The aim of this work is to identify a generic model that could be used in different wind engineering cases in practice. In view of this the wall reflection terms are not included. Discussion on how this may affect the results is included later in the paper. It should be noted that commercial CFD codes tend not to include these terms (CFX 1997, FLUENT 1995).

3. The test case

3.1. Full-scale measurements

A full-scale 6m cube was constructed at the Silsoe Research Institute (Hoxey 1999) in order to compare CFD results with full-scale as opposed to model scale wind tunnel results. The cube is positioned in a boundary layer generated from a fetch consisting of short grass with an effective roughness height of 0.01 m. This is relatively constant as the experimental results are obtained during the winter months when high winds prevail and the grass does not grow. The cube can be rotated through 360° and can be pitched about a horizontal axis. The cube surface consists of sheet metal cladding with a smooth plastic coating to afford protection and avoid changing of the surface roughness due to rust.

Data was obtained from the full-scale cube using a total of 16 pressure taps located at 1m intervals and positioned along the front, roof and rear centreline of the cube, as shown in Fig. 2.

The resulting flowfield is very complicated due to complex strain features arising from curvature, swirl, acceleration, deceleration, separation, reattachment and impingement. The flow field is further complicated by the presence of an unsteady and highly turbulent wake.

3.2. Computational details

The computational domain used is detailed in Fig. 1. In addition a cube skewed at 45° to the incident wind was used.

The sides, lid and most importantly the inlet and outlet of the domain were positioned so as minimise any unphysical interference with the flow field around the cube. Baetke *et al.* (1990) states that the blockage ratio, defined as the ratio of the frontal area of the cube to the vertical cross sectional area of the computational domain should be no greater than 3%. The

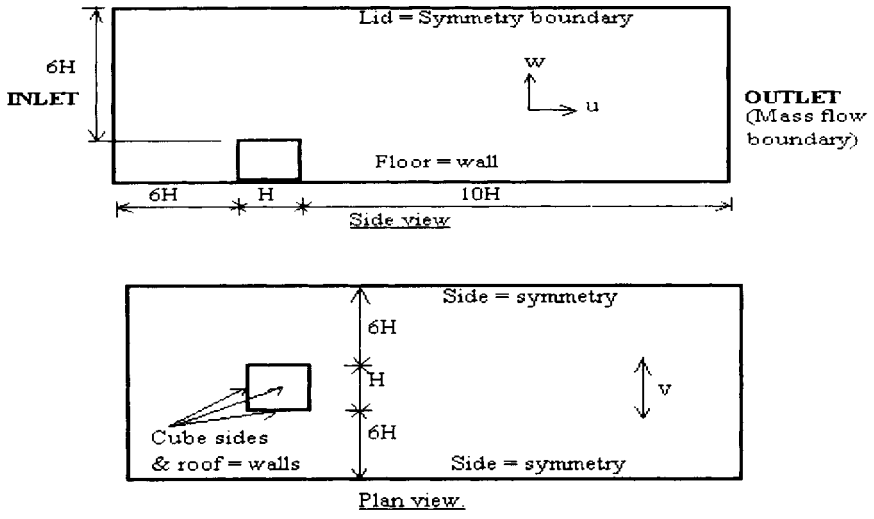

Fig. 1 The computational domain

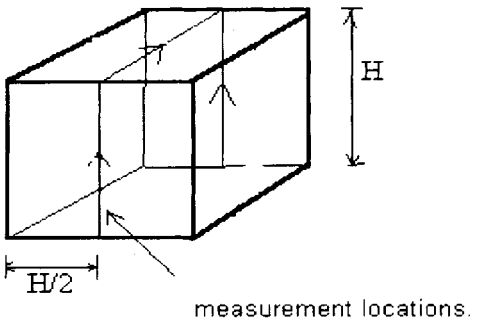

Fig. 2 Cube measurement locations

blockage ratio for these tests was less than half this value. Furthermore flow gradients at the outlet were monitored to determine a suitable length of the computational domain for the wake region so as not to compromise the interior solution accuracy of the simulation. Approximately 120,000 nodes were used in meshing the domain with particular refinement at the areas of flow impingement and separation. Grid independence tests detailed later utilised approximately 550,000 nodes. The solutions were converged until residual reduction factors (the ratio of the residual at the second and last iteration) of 1×10^5 were achieved. This is a more stringent tolerance than would be used in practice, but was felt necessary to allow for firm conclusions to be drawn on the relative merits of the turbulence models.

The floor roughness length was set equal to 0.01 m to represent the fetch at the SRI and the cube walls were given a roughness length equal to 0.005 m. This was done through an amendment to the logarithmic law of the wall. The inlet conditions were generated by running the CFD simulations for flow over rough ground with no building present and periodic streamwise boundary conditions to give a velocity of 10 m/s at the building height. This gave fully developed equilibrium flow profiles including variables such as streamwise velocity and

turbulent kinetic energy that were consistent with the floor roughness. These were used as inlet conditions for simulations with a building in the flow. The results returned by the numerical boundary layer simulations were in excellent agreement with Richards and Hoxey (1993) which details equations that specify the velocity profile and a maximum value of turbulent kinetic energy production at ground level.

Both hybrid (Spalding 1972) and CCCT (Gaskell and Lau 1988) convective differencing were used. The former is commonly used because of its simplicity and stability. However, it suffers from inaccuracies due to its first order accuracy which leads to numerical, false diffusion. CCCT seeks to overcome this by using a higher order interpolation for fluxes combined with an algorithm to prevent unphysical under or over shoots.

4. Preliminary CFD tests

4.1. Discretisation

A number of tests were undertaken, using the RNG k-ε model, to assess the effect of the choice of convective differencing schemes on the CFD flowfield and pressure distributions. The results showed that the use of hybrid differencing had the effect of increasing the turbulence in the flowfield, due to the effects of false diffusion, for both the normal and skewed cube models. On comparison with results obtained from CCCT differencing, this additional false diffusion resulted in an approximate increase in the peak negative pressure at the front corner of the cube of about 10% and a reduction in the length of the roof vortex, for the normal cube orientation, of approximately 5-7%. Therefore it is felt necessary to use higher order convective differencing in wind engineering simulations.

4.2. Grid independence tests

With any CFD simulation it is important to check the results for grid independence. If the results continue to change appreciably as the grid is refined then the results are open to question. Solutions were calculated with the number of cells at 110,000 and 550,000. The

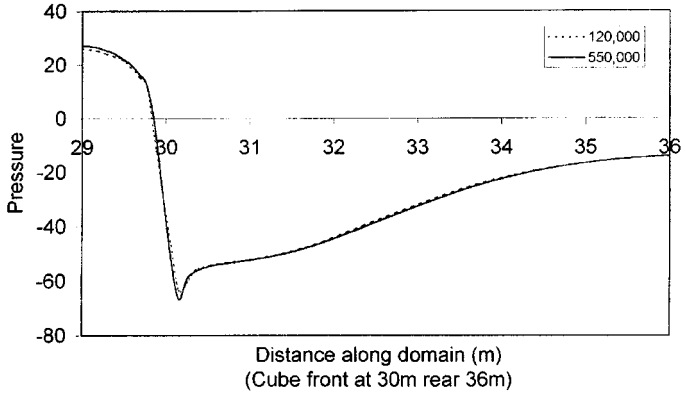

Fig. 3 Roof pressure coefficient distributions for the grid refinement test using the 6m normal cube model (Number of nodes used shown in legend)

results of this can be seen on Fig. 3. It is clear from the results that further flow field changes are minimal upon increasing the grid resolution. Increased grid resolution was only used to aid the convergence of the differential stress model. Checks were also carried out to ensure that values of y^+ for the first grid point from the wall were in the correct range.

5. Results for each turbulence model and comparison with full-scale

All graphs and data presented contain data on the cube centre line (see Fig. 2) unless otherwise stated.

Pressure coefficients are derived by normalising the CFD derived pressure by the calculated dynamic pressure calculated upstream of the cube at 6 m.

5.1. Roof flow field patterns and pressure distributions

Table 1 shows the roof vortex length calculated for the four turbulence models tested. The length of the predicted vortex is a good measure of the accuracy of a simulation. The RNG k-ε model is the only one to predict a reattached vortex. Vector plots of the flow fields on the cube centreline for the four turbulence models are given in Fig. 11 to 14. These demonstrate in more detail the different flowfields predicted. The reasons for this are addressed in the following sections.

5.1.1. k-ε

From comparison with the experimental work conducted by Hoxey (1999) it is apparent that the standard k-ε model has difficulty in predicting the flow fields and pressure distribution around a bluff body. Fig. 4 shows the excessive levels of turbulent kinetic energy produced on the windward face of the normal cube. Contributions from the three normal Reynolds stress turbulence components raise the maximum possible windward face stagnation pressure to a value greater than unity (Fig. 5), which is far in excess of the values from experiment and predicted by Cook (1986). Furthermore the sharp peak and large gradient of the negative pressure behind the upstream edge of the roof (Fig. 6) are caused by the flow not separating which in turn is caused by the overproduction of turbulent kinetic energy at the impinging area and the upstream edge. The overproduction of turbulent kinetic energy and thus eddy viscosity excessively mixes and arrests the vertical flow component and the flow incorrectly remains attached to the roof of the

Table 1 Roof vortex length for cube normal to incident wind

Turbulence model	Roof vortex length
Standard k-ε	None
MMK k-ε	No reattachment
RNG k-ε	0.86H
Differential stress	No reattachment
Experiment (Hoxey 1999)	0.5H-0.6H

Table 2 Wake recirculation lengths for cube normal to the incident wind

Turbulence model	Normalised wake recirculation length
Standard k-ε	2.1
MMK k-ε	3.12
RNG k-ε	2.5
Differential stress	2.1
Experiment (Hoxey 1999)	1.2-1.4

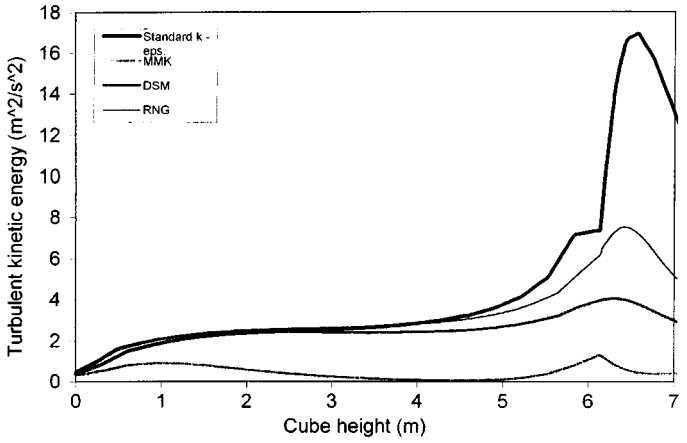

Fig. 4 6 m cube normal to the incident wind, front face centreline turbulent kinetic energy profile

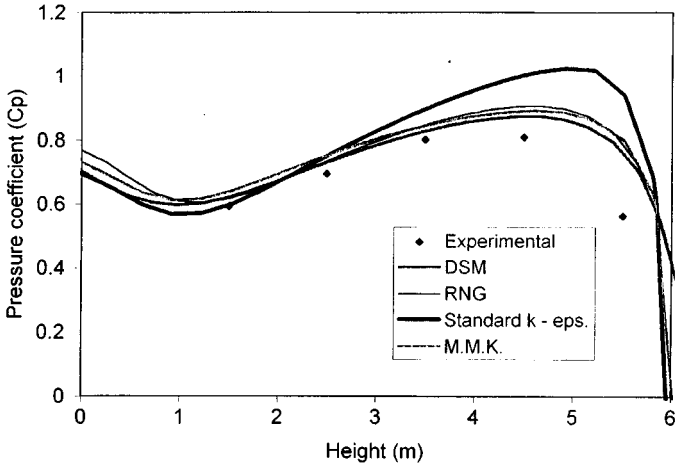

Fig. 5 6 m cube normal to the incident wind, front face centreline pressure coefficient distribution

cube. A similar result was found with the cube skewed at 45 degrees to the incident wind and Fig. 7 shows that the k-ε model predicts the weakest delta wing vortex due to excessive mixing. These results at full-scale are not surprising, as similar effects have been widely reported in comparisons of CFD and wind tunnel measurements (Murakami 1993).

The standard k-ε model over predicts turbulent kinetic energy at the areas where the flow impinges on the windward face due to its inability to deal with irrotational strain. Irrotational strain arises principally in impingement and reattachment zones. As eddy viscosity models have arisen from and been calibrated by reference flows which are strongly sheared they have great difficulty in dealing with flow fields which are dominated by extensive straining (Leschziner 1995). The excessive values of turbulent kinetic energy are caused by overestimation of the turbulence production term, P_k, which in turn is a consequence of the eddy viscosity concept. The isotropic eddy viscosity formulation simply sums the turbulence production due to these terms. Hence eddy viscosity models which feature the turbulence energy transport equation tend to return

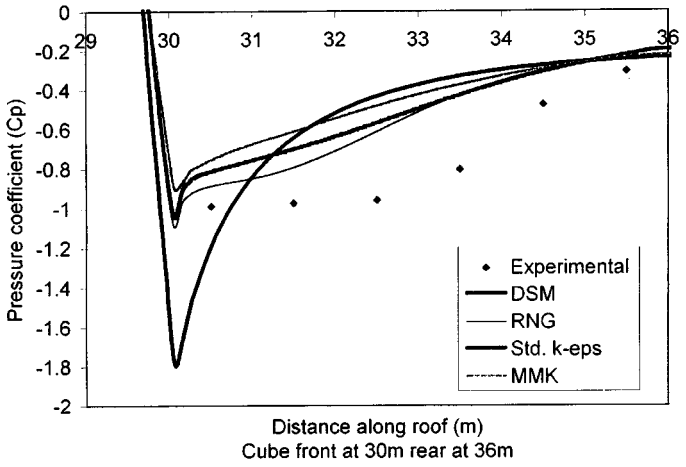

Fig. 6 6 m cube normal to the incident wind, roof centreline pressure coefficient distribution

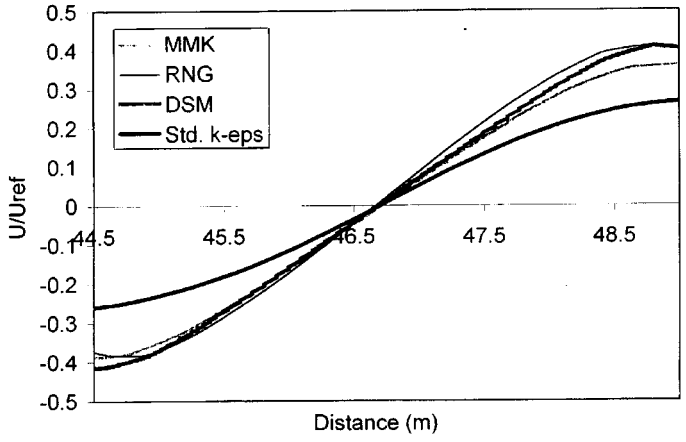

Fig. 7 6 m cube skewed at 45° to the incident wind, roof lateral velocity component to show the relative strength of the predicted delta wing vortex

excessive levels of energy and thus turbulent diffusion in the presence of strong compressive strain.

5.1.2. MMK

The MMK k-ε model shows a very different picture indeed, with flow recirculation occurring over the entire length of the roof with no flow reattachment (Fig. 12). This is in fact an extrinsic three-dimensional effect because, when off-centre planes are viewed, it can be seen that the flow reattaches on the roof. The windward face flow field by contrast appears to be reasonably well predicted with a pressure distribution nearer to full-scale measurements than the standard k-ε model (see Fig. 5) and development of a well-defined frontal vortex. Similar pressure distributions to the RNG model and DSM are predicted for the roof of the cube (Fig. 6).

The MMK k-ε model attempts to reduce the production of turbulent kinetic energy at the front face of the cube. In this work it appears that the model overcompensates as a flow field

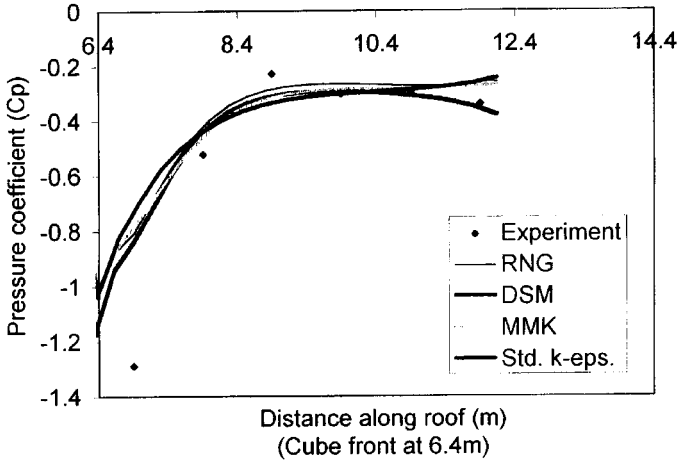

Fig. 8 6 m cube skewed at 45° to the incident wind, roof centreline pressure coefficient distribution

similar to that produced by the standard k-ε model with a vertically uniform incident wind is predicted. The turbulent kinetic energy produced at the front corner now appears to be too small (Fig. 4) and there is no flow reattachment on the roof. Simulations with higher surface roughness values and low inlet velocity were carried out, but reattachment was still not observed. The very low levels of turbulent kinetic energy production at the flow impingement locations appear to contribute to the development of stronger delta wing vortices (Fig. 7) than predicted by the standard k-ε model although only a modest improvement in the roof pressures prediction was apparent (Fig. 8).

5.1.3. RNG

The RNG k-ε model appears to produce good results particularly when compared to the standard k-ε model. It is the only one of the four tested that is able to predict flow separation and reattachment on the roof of the cube (Table 1). This can also be seen in Fig. 13 where the recirculation can be seen by studying the velocity vectors. This also has the effect of reducing the height of the wake recirculation zone compared with MMK k-ε and DSM (Figs. 12 and 14). RNG predicts relatively accurate pressure distributions around the cube on comparison with the experimental results, as shown on Figs. 5 and 6. Referring to Fig. 4 it can be seen that the RNG k-ε model produces three to four times more turbulent kinetic energy at the flow stagnation point than the differential stress model. For the skewed model it predicts stronger roof vortices and a better calculation of the roof pressure coefficients than the standard k-ε model.

There are several reasons for the RNG k-ε model's improvement over the standard k-ε model. The RNG model incorporates revised model constants used to close the transport equations. Furthermore the ε equation now includes a strain dependent term to deal with flows that experience large rates of deformation. Orzag (1994) stated that the reduced value of $C_{\varepsilon 2}$ compared with the equivalent standard k-ε model coefficient has the beneficial consequence of decreasing both the rate of production of k and the rate of destruction of ε, leading to smaller eddy viscosities. Secondly, the strain dependent term in the modified ε equation has the effect of

modifying the rate of dissipation depending on whether the flow is subject to isotropic or strongly anisotropic turbulence. In areas of high straining the strain dependent term increases the production of energy dissipation term in the dissipation equation, the net result of which will be to further reduce the eddy viscosity returned

5.1.4. DSM

The Differential Stress Model (DSM) generally predicts velocities and pressures similar to MMK and RNG. The main differences are for the skewed cube where a delta wing vortex forms on the roof. Fig. 8 shows that DSM captures the drop in pressure at the rear of the cube and Fig. 9 shows DSM as the best fit for pressures on the front face. Table 1 shows that the DSM model fails to predict reattachment of the roof vortex.

Initial assumptions were that the differential stress model would be able to more adequately predict the physics of fluid flow taking full account of the anisotropy of Reynolds stresses and flow history effects in contrast to the k-ε models. Flow features such as streamline curvature which occur with shear layers bordering a separation bubble and irrotational strain in impinging regions of flow have a profound effect on turbulence and are closely associated with anisotropy (Leschziner 1995). Fig. 10 clearly shows the anisotropy of the Reynolds

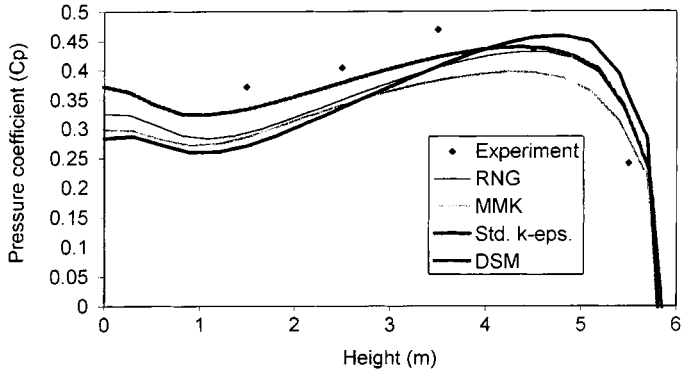

Fig. 9 6 m cube skewed at 45° to the incident wind, front face centreline pressure coefficient distribution

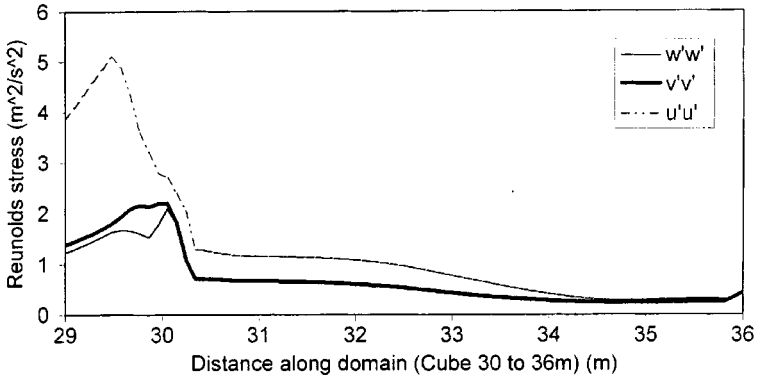

Fig. 10 6 m cube normal to the incident wind, roof centreline Reynolds stress (normal) distribution

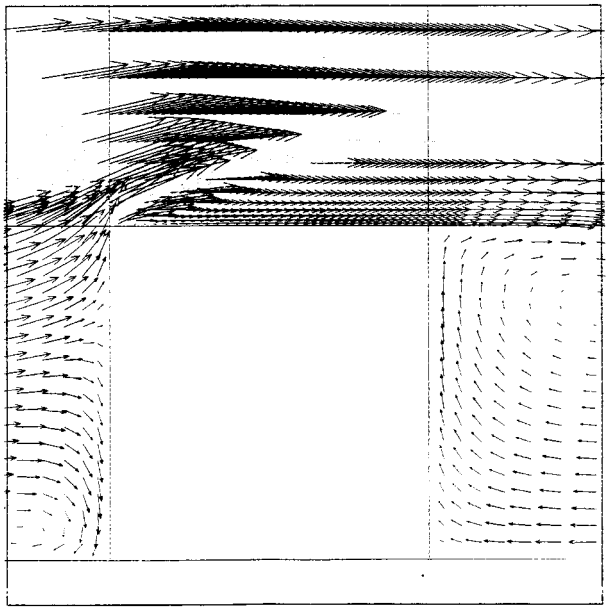

Fig. 11 6 m cube centreline velocity vectors for the standard k-ε turbulence model

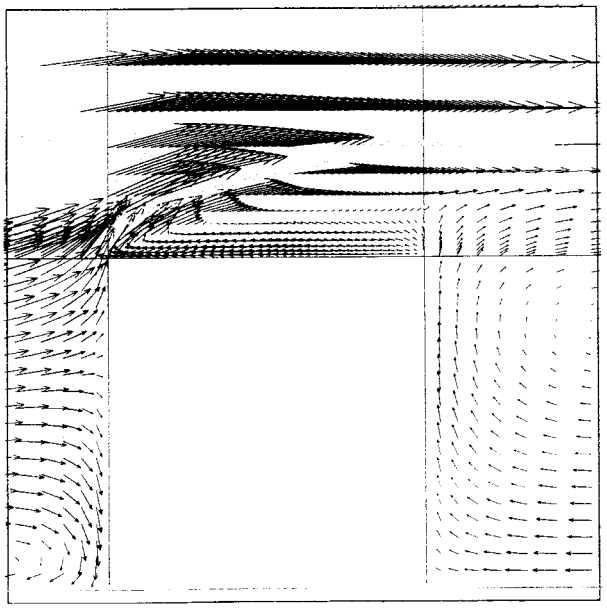

Fig. 12 6 m cube centreline velocity vectors for the MMK k-ε turbulence model

stresses over the roof of the cube model. The stream wise fluctuating velocity component $u'u'$ dominates the stresses, particularly in the region of the roof vortex. The reason for the poor roof flowfield may arguably be due to the omission of wall reflection terms. These terms modify the isotropisation process of the pressure strain term. The increasing anisotropy of

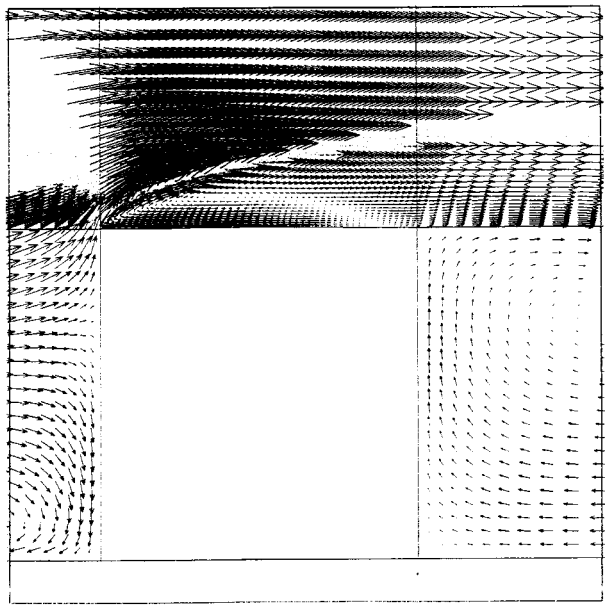

Fig. 13 6 m cube centreline velocity vectors for the RNG k-ε turbulence model

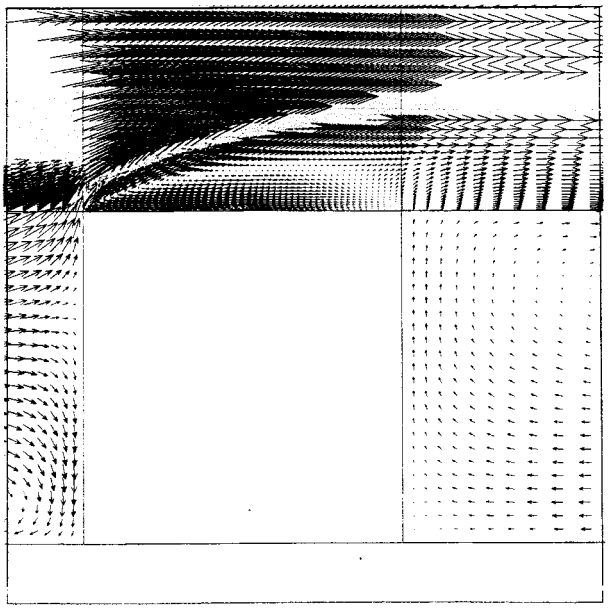

Fig. 14 6 m cube centreline velocity vectors for the differential stress turbulence model

turbulence as solid surfaces are approached tends to decrease normal and increase tangential turbulence intensities thus leading to an increase in the Reynolds stress parallel to the wall. The authors have previously incorporated the Craft and Launder terms into the model but have had no success in running the full 6 m-cube simulation to converged results with the current solution algorithms, which may well be due to the high Reynolds number. Murakami

(1993) has previously undertaken testing of a total of 6 differential stress models, which incorporated different pressure strain models and wall reflection terms for the flow over a wind-tunnel, surface-mounted cube in an atmospheric boundary layer. Although a scale model was used, it was the same general test case as here. The results of these tests showed that even with the extra terms the DSM could not predict a roof vortex reattachment to match experimentally obtained results which showed a vortex reattachment at approximately 2/3rds of the distance along the roof. Nevertheless this model predicted relatively accurate pressure distributions. Relative insensitivity to wall treatments was also described by Hanjalić *et al.* (1998), whose conclusions suggest that wind engineering flows are dominated by the convection and diffusion of large scale eddies and less by the small-scale effects. Therefore wall reflection terms should not have a major effect on the flowfield.

5.2. Wake recirculation zone data

The computed dimensions of the wake vortex provide a further means of assessing the accuracy of a CFD simulation. The following results represent the length of the wake recirculation zone normalised by the cube dimension, H.

It can be seen that the standard k-ε model over predicts the size of the recirculation vortex. As this region exhibits strong turbulence anisotropy where the $v'v'$ lateral Reynolds stress component dominates (Murakami 1993) it is immediately apparent that isotropic eddy viscosity models will not be able to adequately predict the recirculation vortex. This model underestimates the value of $v'v'$ in the wake region and consequently underestimates the momentum diffusion in the lateral direction (Murakami 1993). The net result of this is that the kinetic energy, calculated as the sum of the Reynolds stress, is underestimated and thus the predicted value of eddy viscosity is too small. Insufficient mixing of the flow in the vortex results in an over prediction of the reattachment length and too large a velocity in the reverse flow. Nevertheless this model predicted a smaller recirculation zone than the RNG model. This is probably due to the generally high levels of turbulent kinetic energy surrounding the cube being convected down stream from the upper part of the front face. The RNG model produces reasonably accurate results for the wake recirculation zone considering the lower levels of turbulent kinetic energy predicted by this isotropic turbulence model.

The MMK k-ε model also over predicts the wake recirculation. This model, which is in fact amended to give a higher value of turbulent kinetic energy in the wake region and thus reduce the recirculation length, is somewhat impeded by the errors in the flow field over the roof. The large roof recirculation has the effect of producing a wake recirculation that extends from the base of the cube to the top of the roof vortex. The net effect of this produces a wake recirculation for a cube of larger dimensions than that tested. This emphasises the importance of accurately predicting the correct flow field at all points over the cube due to the interactions of different flow regions.

The differential stress model, due to its ability to determine the anisotropic turbulence properties of the wake region, predicts a more accurate reattachment length.

5.3. Comparison of experimental and computational results

In addition to the above discussion of each model compared to the experimental data, it is

possible draw out a few points from a comparison between the experimental data and the turbulence models generally.

Experimental results are presented alongside the computational results in Figs. 5, 6, 8 and 9. Fig. 5 shows front face centreline pressure coefficients for the case of the normal cube. The results from the best models (MMK, RNG, DSM) are close to the experimental results. The main differences occur higher up the face with a 20-30% difference at the highest part, which demonstrates the problems encountered by all models in this region of high shear stresses. Fig. 6 also shows qualitative agreement with errors of the order of 10% at the front and back of the roof. There is some question over the accuracy of the middle two experimental points. Nonetheless the results here are not as good as might be hoped, although they do display the correct magnitude and trends.

Fig. 8 shows roof centreline pressure distributions for the skewed cube. There is good agreement apart from the first pressure tap near the leading edge. This is likely to be due to the steep gradients in this area and future work will seek to discover whether this can be overcome through highly localised grid refinement. Fig. 9 shows errors of 10% or less for the front face centreline pressures, which is more encouraging than the normal cube results.

6. Conclusions

CFD results were successfully produced for flow around a full-scale, 6 m building. As widely reported elsewhere, the main errors produced by the standard k-ε model were due to overproduction of turbulent kinetic energy at regions of flow impingement due to the isotropic eddy viscosity assumption. The MMK model incorporating revisions to the standard k-ε model gave significant improvement for the pressure distributions, but did not for the flowfield. The RNG k-ε model is able to provide significantly improved flow field and pressure coefficient predictions through minor changes to the standard model equations. However, this improvement was not reflected in the wake length prediction.

The differential stress model appears to have some deficiencies when used in wind engineering flow fields, although the wake recirculation and pressure distributions were reasonably accurate. Unfortunately any improvements in accuracy available with this model have a penalty of lower computational stability and CPU times approximately three times higher than the standard k-ε model.

Based on these results it is recommended that higher order differencing is always used and that grid independence tests are routinely carried out.

Overall it is concluded that anisotropy is a crucial feature in Wind Engineering applications and a successful turbulence model must incorporate this along with numerical stability at high Reynolds number. In view of this the authors are investigating the use of non-linear k-ε models which retain the stability of standard k-ε whilst accounting for turbulence anisotropy.

Acknowledgements

Gary Easom is grateful for support from a joint University of Nottingham/Silsoe Research Institute Ph.D. Studentship.

References

Baetke, F & Werner, H. (1990), "Numerical simulation of turbulent flow over surface mounted obstacles with sharp edges and corners", *Journal of Wind Engineering and Industrial Aerodynamics*, **35**, 129-147, Elsevier, Amsterdam, Netherlands.

Castro, I.P & Robins, A.G. (1977), "The flow around a surface mounted cube in a uniform & turbulent shear flow", *J. of Fluid Mech.*, **79**, 307-335.

CFX International, Harwell. (1997), UK, '*CFX-4.2 User Manual*'.

Cook, N.J. (1986), "The designers guide to wind loading on building structures part 1", Butterworths, London, England.

Easom, G.J. (1997), "Improved computational models for wind engineering", Internal Report No. FR97 016, School of Civil Engineering, The University of Nottingham, U.K.

FLUENT Inc. (1995), '*FLUENT User Manual*'.

Gaskell, P.H. & Lau, A.K.C. (1988), "Curvature compensated convective transport: SMART, A new boundedness preserving transport algorithm", *Int. J. Num. Meth. in Eng.*, **8**, 617-641.

Hanjalić, K., Obi, S. and Hadžić, I. (1988), "Wall-jets and flows over wall-mounted cubical obstacles", *6th ERCOFTAC/IAHR/COST Workshop on Refined Flow Modelling.*

Hoxey, R.P, Private Communication, 1999.

Launder, B.E & Spalding, D.B. (1974), "The numerical computation of turbulent flows", *Comput. Methods Appl. Mech. Eng.*, **3**, 269-289.

Launder, B.E., Reece, G.J. & Rodi, W. (1975), "Progress in the development of a Reynolds stress turbulence closure", *J. Fluid Mech.*, **68**, 537-566.

Leschziner, M.A. (1995), "Modelling turbulence in physically complex flows", *Industrial Hydraulics and Multiphase flows - Hydro 2000*, Thomas Telford, London, England.

Murakami, S. (1993), "Comparison of various turbulence models applied to a bluff body", *Journal of Wind Engineering and Industrial Aerodynamics*, **46 & 47**, 21-36, Elsevier, Amsterdam, Netherlands.

Murakami, S., Mochida, A. & Ooka, R. (1993), "Numerical simulation of flowfield over a surface-mounted cube with various second-moment closure models", *Ninth Symposium on turbulent shear flows*, Kyoto, Japan.

Murakami, S. (1997), "Overview of turbulence models applied in CWE", Institute of Ind. Science, Univ. Tokyo, Japan.

Orzag, S.A (1994), Lecture notes of ICASE/LaRC short course on Turbulence Modeling & Prediction, March 1994 in Gatski T.B, Hussaini M.Y & Lumley J.L 1996, "Simulation and modeling of turbulent flows", Oxford University Press, Oxford, England.

Patankar, S.V. and Spalding, D.B. (1972), "A calculation procedure for heat, mass and momentum transfer in three-dimensional parabolic flows", *Int. J. Heat Mass Transfer*, **15**, 1787.

Richards, P.J. and Hoxey, R.P. (1993), "Appropriate boundary conditions for computational wind engineering models using the k - ε turbulence model", *Journal of Wind Engineering and Industrial Aerodynamics*, **46-47**, 145-153.

Smagorinsky, J.S. (1963), "General circulation experiments with primitive equations, Part 1; basic experiments", *Mon. Weather Rev.*, **91**, 99-164.

Spalding, D.B (1972), "A novel finite difference formulation for differential expressions involving both the first and second derivatives", *Int. J. Numerical Methods in Eng.*, **4**, 551.

Speziale, C.G (1994), Lecture notes of ICASE/LaRC Short course on Turbulence Modeling & Prediction, March 1994 in Gatski T.B, Hussaini M.Y & Lumley J.L 1996, '*Simulation and Modeling of Turbulent Flows*', Oxford University Press, Oxford, England.

Stone, H.L. (1968), "Iterative solution of implicit approximations of multidimensional partial differential equations", *SIAM J. Numer. Anal.* **5**(3), 530-558.

Tsuchiya, M., Murakami S., Mochida, A., Kondo, K. & Ishida, Y. (1996), "Development of a new k-ε model for flow & pressure fields around a bluff body", *CWE96, Second International Symposium on CWE*, Colorado State University, U.S.A.

Webster, R (1998), "Efficient algebraic multigrid solvers with elementary restriction and prolongation", *Int. J. Num. Meth. in Fluids*, **28**(2), 317-336.
Williams, C.W & Baker, C.J. (1990), "Appraisal of a semi-empirical model for the pressure field beneath roof corner vortices", Department of Civil Engineering, University of Nottingham, U.K.
Yakhot, V., Orzag, S.A, Thamgam, S., Gatski, T.B. & Speziale, C.G. (1992), "Development of turbulence models for shear flows by a double expansion technique", *Physics of Fluids: A: Fluid Dynamics*, **4**(7), 1510-1520.

Notations

U_i	*i*th component of velocity
U_{ref}	reference velocity, taken here at a height of 6 m.
k	turbulent kinetic energy, $k = 1/2\,(u'_i u'_i)$
ε	dissipation rate of k
P	pressure
ρ	fluid density
τ_{ij}	Reynolds stress tensor
σ_k, σ_ε	Turbulent Prandtl number for k and ε for the k-ε turbulence model
μ_t	dynamic eddy viscosity
ν_t	kinematic eddy viscosity
S_{ij}	strain rate tensor
δ_{ij}	Kronecker delta
$\overline{u_i' u_j'}$	Reynolds stresses
P_k	Production of k
$C_{\varepsilon 1}$, $C_{\varepsilon 2}$, $C_{1\text{RNG}}$, C_μ	constants in the turbulence transport equations
Ω	vorticity
S	shear
C_{ij}	convection term of $\overline{u_i' u_j'}$
D_{ij}	diffusion term of $\overline{u_i' u_j'}$
F_{ij}	stress production of $\overline{u_i' u_j'}$ by action of rotational or body forces
ϕ_{ij}	pressure-strain correlation term
ε_{ij}	dissipation term of $\overline{u_i' u_j'}$

(*Communicated by Giovanni Solari*)